Available online at www.sciencedirect.com
ScienceDirect
Polymer 48 (2007) 2619–2635
polymer
www.elsevier.com/locate/polymer

Experimental analysis and simulation of the gas transport in dense Hyflon® AD60X membranes: Influence of residual solvent

Marialuigia Macchione [a,b], Johannes Carolus Jansen [a,*], Giuseppina De Luca [b], Elena Tocci [a], Marcello Longeri [b], Enrico Drioli [a,c]

[a] *Institute on Membrane Technology ITM-CNR, University of Calabria, 87030 Rende (CS), Italy*
[b] *Department of Chemistry, University of Calabria, 87030 Rende (CS), Italy*
[c] *Department of Chemical Engineering and Materials, University of Calabria, 87030 Rende (CS), Italy*

Received 19 December 2006; received in revised form 28 February 2007; accepted 28 February 2007
Available online 3 March 2007

Abstract

The present paper discusses the tendency of solution-cast Hyflon® AD membranes to retain unexpectedly high amounts of solvent, the possible reasons of this phenomenon and its effect on the membrane performance. Dense membranes, prepared by solution-casting and subsequent evaporation, showed large differences in their thermal, mechanical and transport properties, depending on the residual solvent content. Complete solvent removal required heating under vacuum up to well above the glass transition temperature. Analysis of the permeability, diffusion and solubility coefficients of six permanent gases showed that plasticization by the residual solvent reduces the permselectivity and increases the permeability.

Data of solution-cast membranes after complete solvent removal compare well with those of a melt-pressed sample. Experimental gas transport parameters were confronted with simulated data, obtained by the Gusev–Suter Transition-State Theory (TST) method and by molecular dynamics (MD) simulations. ^{1}H High Resolution Magic Angle Spinning Nuclear Magnetic Resonance spectroscopic analysis of the residual solvent in the polymer matrix did not reveal a particular interaction between polymer and solvent, suggesting that the solvent retention is mainly diffusion controlled.

Keywords: Hyflon AD60X; Gas separation membrane; Residual solvent

1. Introduction

Hyflon AD60X is an amorphous perfluorinated copolymer of tetrafluoroethylene (TFE) and 2,2,4-trifluoro-5-trifluorometoxy-1,3-dioxole (TTD) in the molar ratio of 40:60 (Scheme 1). This specific grade has a glass transition temperature, T_g, of about 130 °C and is part of a wider family of copolymers with different molar ratios of the two monomeric units TTD and TFE. These polymers have a similar high thermal, chemical, ageing, weathering and solvent resistance which are characteristic for perfluoropolymers (PFPs), like for instance polytetrafluoroethylene (PTFE). In contrast to the semi-crystalline PTFE, Hyflon polymers are amorphous glasses with a modestly high T_g, as a result of the bulky TTD units in the polymer chain. These amorphous glassy PFPs, such as

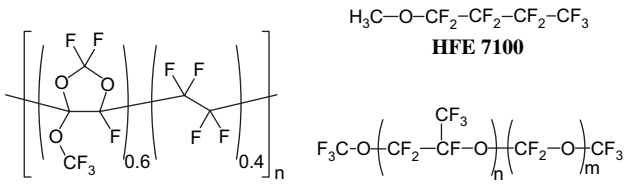

Hyflon AD 60X **Galden HT**

Scheme 1. Chemical structure of the repeating unit in Hyflon AD60X and of the solvents, Galden HT and HFE 7100.

* Corresponding author. Tel.: +39 0984 492031; fax: +39 0984 402103.
E-mail address: jc.jansen@itm.cnr.it (J.C. Jansen).

0032-3861/$ - see front matter © 2007 Elsevier Ltd. All rights reserved.
doi:10.1016/j.polymer.2007.02.068

also those of the Teflon® AF family, are known for their high Fractional Free Volume (FFV) [1] or high void fraction, which is the reason for their exceptional gas permeability [2–4]. The void fraction, reported for Hyflon AD polymers is 9.4–9.5%, against 14.8 and 17.7 for Teflon AF 1600 and Teflon AF 2400, respectively [5]. The reported FFV of Hyflon AD60X of 23% [6] is considerably lower than that of Teflon AF (30% for Teflon AF 1600 and 33% for Teflon AF 2400) [7] but still much higher than that of common polymers like polysulfone, poly(ether sulfone) and polyimide [8]. As a consequence, Hyflon membranes have a relatively high permeability to gases and they are therefore suitable for preparing dense gas separation membranes [6,7,9–11]. Hyflon AD60X forms an attractive compromise of a moderately high selectivity and a still interesting permeability, in comparison with the more permeable but less selective Teflon AF polymers.

Due to their good solvent resistance [2,10] PFP membranes can be applied in fields where condensable species in the gas stream would seriously compromise the performance of the traditional polymers as a result of plasticization [12–14]. The low solubility of common organic liquids in the PFPs, and the consequent lack of swelling of the polymer matrix, makes these polymers not only more resistant but also relatively impermeable to most organic vapours. An exception is formed by some halogenated compounds, enabling the use of PFP membranes for pervaporative removal of CFCs from waste streams [15,16], and of course by fluorinated compounds, which act as solvents or plasticizers for these polymers.

Recently we have shown that Hyflon AD60X has an unusual tendency to retain its own solvent, Galden® HT 55, used when preparing membranes by solution-casting and solvent evaporation, in spite of the low boiling point and high volatility of the solvent [17]. It was found that membranes may contain over 10% of residual solvent, even after extensive drying at 90 °C. One of the immediate effects of the residual solvent was that it reduced the thermo-mechanical stability of the membrane by plasticization of the polymer, and that it caused foaming of the solution-cast film upon rapid heating under vacuum. Furthermore, it decreased the permselectivity of the membranes and increased the gas permeability and the diffusion coefficients of especially the larger gas species. Besides the influence of residual solvent on the instantaneous properties, the possibility that this solvent is gradually released during membrane operation introduces a potential time dependence of the membrane performance. Such time dependence is generally undesired in any kind of industrial separation processes, where stable operation is one of the most important requirements. Therefore knowledge of the amount of residual solvent in as-cast membranes, of its effect on the membrane performance and of possible methods to realize its complete removal is very important.

The effect of residual solvent on the performance of dense membranes has been studied by several authors, often in relation to the membrane preparation conditions. In general, the solvents used during the casting procedure, may have a considerable influence on the gas transport properties [18,19]. A study on 6FDA–*m*PDA polyimide films shows that the transport parameters are greatly affected by the presence of residual solvent: the diffusion coefficient decreases with decreasing residual solvent content, whereas the permeability and solubility coefficients increase [18]. Another study conducted by Maeda showed that melt extruded polysulfone films had between 10% and 20% lower gas permeabilities than solution-cast polysulfone films [20]. This may be due to orientation in the former and due to residual solvent in the latter. The same experimental evidence was obtained by Pinnau and Toy [3] with Teflon AF 2400. Their permeability coefficients and selectivities of a solvent-cast Teflon AF 2400 film were compared to those reported by Nemser and Roman for a melt-pressed membrane [21]. The permeabilities of the solution-cast film were between 30% (helium) and 80% (methane) higher than those reported for the melt-pressed film. Comparing literature data of polycarbonate membranes prepared under different conditions, Hacarlioglu et al. found differences of over 400% in the nitrogen permeability coefficient, depending also on the amount of residual solvent and on its removal procedure [19]. In qualitative terms the effect of the residual solvent is often ascribed to specific changes in the polymer state or morphological aspects such as the surface roughness [22], to variations of the free volume of the polymer [23] or to changes in the polymer chain conformation [19,24–26]. Only in a few occasions the amount of residual solvent has been quantified. The absolute value usually depends on the membrane preparation procedure [19] and on the solvent type, but even for low-volatile solvents it generally does not exceed a few percent [18].

In this light the remarkable solvent retention observed in Hyflon AD60X membranes seems particularly interesting, the more so because the polymer's high FFV is supposed to facilitate mass transport. In the previous paper [17] it was hypothesized that the solvent retention could be related to diffusion phenomena, to the particular free volume distribution of Hyflon or to specific polymer–solvent interactions. The aim of the present paper is to present the first systematic study on this phenomenon and on the effect of residual solvent in high free volume perfluorinated polymers. The paper will focus in particular on two different fluorinated solvents and their effect on the physical and transport properties of Hyflon AD60X membranes, studied by means of Differential Scanning Calorimetry (DSC) and gas permeation measurements. The transport properties of the solution-cast membranes are also compared with those of a solvent-free melt-pressed sample. The paper will further describe a non-destructive procedure for complete solvent removal and for quantification of the solvent content. The presence of the solvent is further studied by solid-state NMR analysis of the samples, providing information on the physical state of the solvent in the polymer matrix and on possible polymer–solvent interactions. Finally, the possibility to model the gas transport by molecular simulation studies is evaluated. Experimental results are confronted with simulated data, obtained using the Gusev–Suter Transition-State Theory (TST) [27] method and using MD simulations. The advantages and limitations of TST and MD will also be discussed.

2. Experimental section

2.1. Materials

Hyflon AD60X (Scheme 1), an amorphous TTD–TFE copolymer containing 60 mol% 2,2,4-trifluoromethoxy-1,3-dioxole (TTD) and 40 mol% tetrafluoroethylene (TFE), was kindly supplied by Solvay-Solexis. Hyflon AD60X has a reported density of 1.93 g/cm^3 at 20 °C [6]. This polymer shows excellent resistance to organic solvents; the only known solvents are perfluorinated compounds. In this study 1-methoxy-nonafluorobutane (3M, commercial name HFE 7100, Bp 60 °C, MW 250 g/mol) and Galden HT 55 (Solvay-Solexis) were used as the solvents to prepare the solution-cast membranes (Scheme 1). Galden HT is a mixture of oligomeric perfluoropolyethers of which molar mass depends on its specific grade. Galden HT 55 has a boiling point of 55 °C and an average molar mass of 350 g/mol [28].

2.2. Membrane preparation

Dense Hyflon AD60X gas separation membranes were prepared by the solvent evaporation method from a 5 wt% polymer solution in a Petri dish, using Galden HT 55 or HFE 7100 as the solvent. The films were first dried overnight at room temperature and then in a vacuum oven with very slow heating from 50 to 200 °C at 0.02 °C/min, in order to allow slow evaporation of the solvent without foaming. A previously described dense membrane, prepared without the use of a solvent by melt pressing of the polymer powder, was used as a reference [17]. An overview of the membranes and the fundamental differences in their preparation is given in Table 1.

2.3. Gravimetric measurements

In order to quantify the amount of residual solvent and to determine its release rate, a membrane sample was heated slowly in a vacuum oven and its weight was measured periodically. For each weighing the vacuum was temporarily released and the sample was removed from the oven. This operation took only a few minutes and did not interfere significantly with the drying procedure. At various stages of the drying procedure small samples were taken for thermal analysis.

Table 1
Membranes and their main preparation conditions

Membrane	Casting solvent	Treatment	Thickness (μm)
H25	HFE 7100	Dried at room temperature	67.7
H200[a]	HFE 7100	Dried at 200 °C	68.3
G25	Galden HT 55	Dried at room temperature	60.6
G200[b]	Galden HT 55	Dried at 200 °C	65.2
M170	–	Melt pressed at 170 °C	220

[a] Same membrane as H25, after drying under vacuum at 200 °C.
[b] Same membrane as G25, after drying under vacuum at 200 °C.

2.4. Differential Scanning Calorimetry (DSC)

Thermal properties of the Hyflon AD60X virgin polymer and that of the solution-cast membranes, at the different stages of the drying process, were evaluated by DSC analysis. Measurements were carried out on a Pyris Diamond Differential Scanning Calorimeter (Perkin–Elmer). Samples of about 8–15 mg were subjected to a heating/cooling/heating cycle at a rate of 15 °C/min in the range of 50–150 °C. An empty pan with two covers was used as the reference. The effect of the solvent was evaluated on the basis of the first heating run while the difference between the first and the second heating run was used to verify the additional solvent loss upon heating. The glass transition temperature was determined as the *half-c_p extrapolated* value, i.e. the temperature corresponding to half of the c_p increase of the complete transition, calculated by baseline extrapolation before and after the glass transition.

2.5. ^{1}H High Resolution Magic Angle Spinning Nuclear Magnetic Resonance (^{1}H HRMAS NMR)

The presence of solvent in the polymer was also studied by ^{1}H HRMAS NMR. A membrane specimen was cut into thin slices, and about 20 mg of polymer was packed into a 4 mm MAS zirconium rotor of 50 μl total volume, with hemispherical inserts. All HRMAS NMR spectra were recorded at 298 K on a Bruker Avance 500 MHz instrument working at 11.74 T, using a 4 mm HRMAS ^{1}H/^{13}C probe head. The sample was spun at 8000 Hz; a 10 μs 90° pulse, a spectral width of 40 000 Hz and a recycle time of 2 s were used. The free induction decays were stored in 32k words of computer memory. Different spectra of the same membrane were recorded to monitor the solvent evaporation during the thermal treatment.

2.6. Mechanical testing

Tensile tests were carried out on a Zwick/Roell universal testing machine, single column model Zwicki Z2.5, equipped with a 50 N maximum load cell and with pneumatic sample grips with a flat sanded stainless steel surface. The membrane samples were cut into test strips of 10.0 mm wide with an extremely sharp cutter in order to limit as much as possible craze formation during cutting. The specimen thickness was measured with a digital micrometer (Carl Mahr) in at least 5 points and then averaged. Specimens with a thickness variation of more than 5% were discarded. The effective sample length (grip to grip distance) was normally 50 mm and the test speed was 5 mm/min (corresponding to 10% deformation per minute). The test specimens were stretched with a pre-load of 0.2–0.3 MPa before the start of the measurements.

The tensile tester was controlled and the stress–strain curves were recorded and elaborated by the Zwick/Roell *Master TestXpert* software. At least 2–5 different specimens of each membrane sample were tested. Clearly failed measurements were excluded from the statistical analysis.

2.7. Density measurement

The density of a solvent-free sample was determined by the buoyancy method, measuring the weight of the sample specimen in air, m, and immersed in a non-absorbing liquid with a known density (m_{immersed}). The observed weight difference is due to the buoyancy and is the product of the sample volume (V_{pol}) and the solvent density (ρ_{solv}):

$$\Delta m = m - m_{\text{immersed}} = \rho_{\text{solv}} V_{\text{pol}} \quad (1)$$

After elimination of the unknown sample volume, $V_{\text{pol}} = m/\rho_{\text{pol}}$, the polymer density can easily be calculated as follows:

$$\rho_{\text{pol}} = \frac{m\rho_{\text{solv}}}{m - m_{\text{immersed}}} \quad (2)$$

2.8. Gas permeation measurements

Low pressure single gas permeation experiments were carried out in a fixed volume/pressure increase instrument, constructed by GKSS (Geesthacht, Germany) and schematically displayed in Fig. 1. The fixed feed volume of the instrument is about 2 l; the fixed permeate volume is 75.5 cm^3 and is expandable, if necessary, in the case of high fluxes or long measurement times, to reach steady state. Up to eight gas cylinders are connected simultaneously to the instrument and an additional liquid flask can be connected for vapour transport measurements. A feed pressure up to 1.33 bar can be used and the actual value is read with a resolution of 0.1 mbar; the permeate pressure is measured in the range of 0–13.3 mbar with a resolution of 0.001 mbar. The membrane cell diameter is 75 mm but the effective area can be reduced by the use of appropriate masks on the membrane. The entire system is computer controlled: the feed gas pressure is set by pneumatic valves and the gases can be alternated automatically. The instrumental time lag is less than 0.05 s, so time lags down to 0.5 s can be determined with less than 10% error. The crucial parts of the setup are placed in a thermostatic chamber which allows measurements according to a previously chosen temperature program. Feed pressure, permeate pressure, temperature and the automatically calculated permeance are continuously registered during each measurement run and are exported automatically to an Excel data file.

In the present work the membranes were tested over an effective surface area of 11.3 cm^2. Measurements were carried out at 25 °C and at a feed gas pressure of 1 bar. Before the first measurement the membrane cell was evacuated for sufficient time (10–20 min) with a two-stage rotary pump in order to remove dissolved gases or vapours from the membrane and from the rubber seals. Between two subsequent gases the system was evacuated, flushed with the second gas and evacuated again in order to guarantee complete removal of the previous gas.

The measurement of the transport parameters is based on the determination of the pressure increase rate of the fixed permeate volume upon exposure of the membrane to the pure gas.

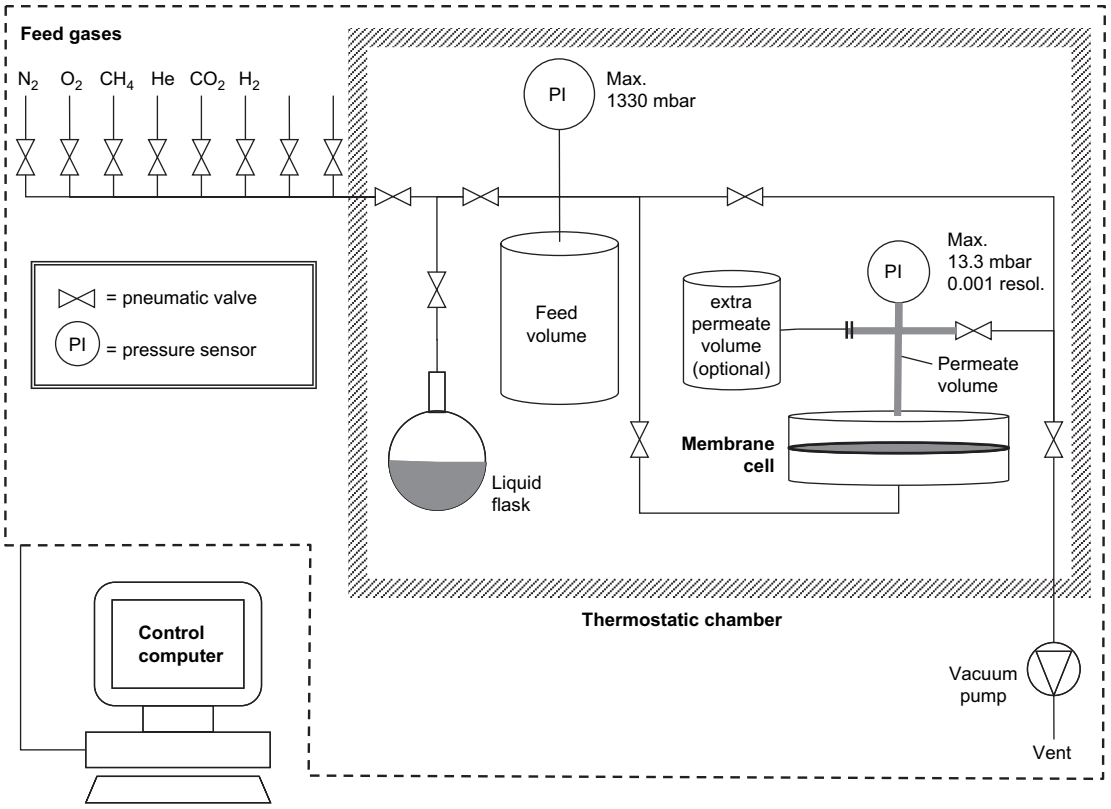

Fig. 1. Experimental setup for the pure gas permeation measurements in the fixed volume/pressure increase mode.

For a constant permeate volume and a constant feed pressure and in the absence of a time lag the permeate pressure will increase asymptotically to the feed pressure, as shown in Fig. 2. If a closed feed volume is used then the feed pressure decreases according to the amount of permeating gas. However, if the feed volume is much larger than that of the permeate, and the feed pressure is much higher than that of the permeate, then a constant feed pressure can be assumed. In that case the permeance, defined as the gas volume (m^3_{STP}) which penetrates a certain membrane area (m^2) per unit time (h) at a given pressure difference (bar), can be calculated from the permeate pressure increase according to the following equation:

$$P = \frac{3600 V_p V_m}{RTAt} \ln\left(\frac{p_F - p_0}{p_F - p_{P(t)}}\right) \quad \text{in} \quad \frac{m^3_{STP}}{m^2\ h\ bar} \tag{3}$$

in which V_P is the permeate volume [m^3], V_m is the molar volume of a gas at standard temperature and pressure [22.41×10^{-3} m^3_{STP}/mol at 0 °C and 1 atm], R is the universal gas constant [8.314×10^{-5} m^3bar/(mol K)], T is the absolute temperature [K], A is the exposed membrane area [m^2], t is the measurement time [s], p_F is the feed pressure and p_0 and $p_{P(t)}$ are the permeate pressures at $t = 0$ and at $t = t$, respectively. The number 3600 is the conversion factor for time [s/h].

If the permeate pressure and the total permeate pressure change is very small and negligible compared to the feed pressure, the logarithmic term in Eq. (3) simplifies to:

$$\ln\left(\frac{p_F - p_0}{p_F - p_{P(t)}}\right) = \ln\left(1 - \frac{p_0 - p_{P(t)}}{p_F - p_{P(t)}}\right) \approx -\frac{p_0 - p_{P(t)}}{p_F - p_{P(t)}} \approx \frac{p_{P(t)} - p_0}{p_F} \quad \text{for } p_0 \text{ and } p_{P(t)} \ll p_F \tag{4}$$

This is generally the case in our measurements, with $p_F \approx 1$ bar and p_0 and $p_{P(t)} < 13$ mbar, and Eq. (3) can thus be approached by a linear equation:

$$P = \frac{3600 V_P V_m}{RTAt} \frac{p_{P(t)} - p_0}{p_F} \tag{5}$$

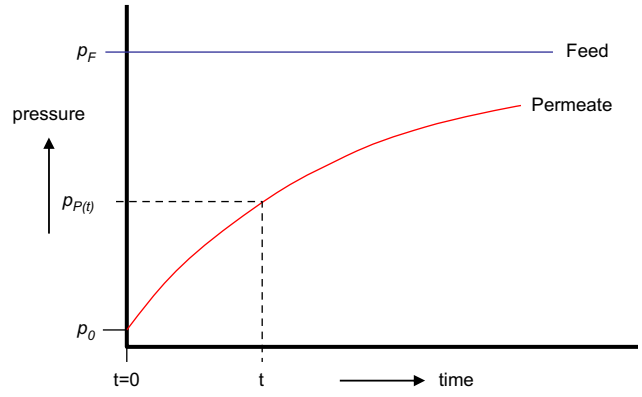

Fig. 2. Permeate pressure increase curve described by Eq. (3) for a membrane system with a constant feed pressure and a fixed permeate volume.

In the initial linear part of the pressure increase curve (Fig. 2) the permeance is proportional to the curve slope or permeate pressure increase rate, dp_P/dt, and can thus be calculated straightforwardly by:

$$P = \frac{3600 V_P V_m}{RTAp_F} \frac{dp_P}{dt} \tag{6}$$

2.8.1. Solubility and diffusion coefficient

Penetrant transport through a polymer film is commonly described by a three-step solution-diffusion process, characterized by absorption of the gas at the polymer–gas interface at the feed side, followed by diffusion of the dissolved species across the membrane and desorption of the gas species from the polymer–gas interface at the low pressure side. In simple cases where the unidirectional penetrant flux obeys Fick's law and where the downstream pressure is negligible compared to the upstream pressure, the permeability is generally expressed as the product of solubility and diffusion:

$$P = DS \tag{7}$$

where D is the diffusion coefficient (cm^2/s) and S is the solubility coefficient (cm^3_{STP}/(cm^3 bar)). The pure gas selectivity, α, is a measure of the potential separation characteristics of the membrane material. It is defined as the ratio of the permeability coefficients of pure gases A and B:

$$\alpha_{A/B} = P_A/P_B \tag{8}$$

Considering Eq. (7), the selectivity can be expressed by:

$$\alpha_{A/B} = (D_A/D_B)(S_A/S_B) \tag{9}$$

The selectivity is clearly the product of two contributions. The first is the ratio of the diffusion coefficients and is often called the mobility or diffusivity selectivity; the second contribution is the sorption selectivity or solubility selectivity and reflects the relative sorption of the gases in the polymer matrix.

Eqs. (7)–(9) define the three fundamental transport parameters in a dense polymeric membrane: permeability, solubility and diffusivity. If the gas solubility is determined independently, for instance by sorption measurements, then Eq. (7) allows the calculation of the diffusion coefficient from permeation data. Alternatively, measurement of P and D allows the calculation of the solubility of the gas in the polymer matrix. A common procedure to determine the diffusion coefficient by permeation experiments is the time-lag method, based on the penetration theory. If a penetrant-free membrane is exposed to the penetrant at the feed side at $t = 0$ and the penetrant concentration is kept very low at the permeate side, then the total amount of penetrant, Q_t, passing through the membrane in time t is given by [29]:

$$\frac{Q_t}{lc_i} = \frac{Dt}{l^2} - \frac{1}{6} - \frac{2}{\pi} \sum_1^\infty \frac{(-1)^n}{n^2} \exp\left(-\frac{Dn^2\pi^2 t}{l^2}\right) \tag{10}$$

in which c_i is the penetrant concentration at the membrane interface at the feed side and l is the membrane thickness. At

long times the exponential term approaches to zero and Eq. (10) reduces to:

$$Q_t = \frac{Dc_i}{l}\left(t - \frac{l^2}{6D}\right) \tag{11}$$

A plot of Q_t versus time describes a straight line which intersects the time axis at $t = l^2/6D$, defined as the time lag, Θ.

$$\Theta = \frac{l^2}{6D} \tag{12}$$

In the setup of Fig. 1 the pressure of the fixed permeate volume is proportional to the amount of penetrant permeating through the membrane and the equation describing the pressure increase takes the same form as Eq. (10) (Fig. 3). If the permeate pressure is again negligible compared to the feed pressure, then Eq. (5), after some rearrangement and introduction of the time lag describes the steady state permeate pressure increase as follows:

$$p_{P(t)} - p_0 = \frac{RTAp_F S}{3600 V_P V_m} D(t - \Theta) \tag{13}$$

The time lag can thus be obtained by linear extrapolation of the steady state pressure increase curve to the time axis or to the starting pressure (Fig. 3). Knowing the membrane thickness, the diffusion coefficient can then be obtained from Eq. (12) and subsequently the solubility can be obtained from the steady state permeation and Eq. (7): $S = P/D$.

2.9. Modelling of transport properties

2.9.1. Generation and equilibration of polymer structures

The TTD and TFE repeating units of Hyflon have been constructed using the Builder module of Insight II [30] employing the COMPASS (condensed-phase optimized molecular potentials for atomistic simulation studies) force field [31] to compute interatomic interactions. The comonomer units were minimised for about 500 iteration steps utilising the steepest-descent and conjugate gradient algorithms. Then a single copolymer chain of 770 repeat units with the appropriate molar ratio of TTD and TFE was constructed, using conditional statistics with the Polymerize module [30]. Since the experimental reactivity ratios for TTD and TFE were not available, a linear chain was constructed by trial and error until the obtained composition (60 ± 1 mol% of TTD) was sufficiently close to the specified composition of Hyflon AD60X. The resulting copolymer chain, with a total of about 7800 atoms, was packed into a cubic box with periodic boundary conditions (PBC) and the dimensions of the box were calculated in such a way that the calculated density of the copolymers corresponded to the experimental value. Three independent initial configurations were generated for each copolymer. Then the backbone dihedral angles were set randomly and the polymer chains were minimised for 300 steps. For the construction of periodic cells a correct distribution of conformational angles and global chain geometry was requested. Based on the Rotational Isomeric State (RIS) model the stepwise chain construction scheme of the Amorphous Cell Program of Insight II [30] was employed to generate the initial structure [32,33].

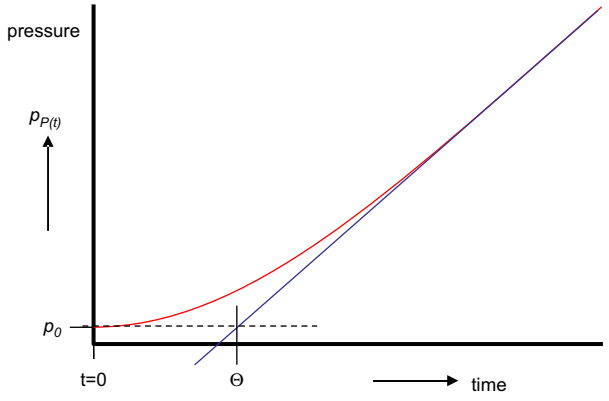

Fig. 3. Time-lag curve for a membrane system with a fixed permeate volume, valid in the case of $p_0 \approx 0$ and $p_{P(t)} \gg p_F$. The steady state curve (tangent line) is described by Eq. (13).

In order to minimize chain end effects, each cell contains only one minimised polymer chain rather than several chains confined to the same volume, which would lead to increased density of chain ends. Fig. 4 shows schematically the packing procedure from a single polymer chain to a fully equilibrated three-dimensional box. The details of the chosen procedure were as follows: the volume of the initial models was chosen in such a way that the packing density was at 85% of the experimental value. The polymer chain and several spacer molecules were packed in the amorphous cell to avoid the artefacts of concatenated rings or a spearing of backbone chains through ring sub-structures. The spacers, e.g. 200 methanol molecules or 200 argon atoms, were added randomly in the simulation box before the packing of the polymer was started and subsequently removed during the equilibration of the polymer models. Also the penetrant gas molecules (10 oxygen, 10 nitrogen and 10 helium molecules) were randomly inserted at energetically feasible positions in this stage of the preparation of the models. The increased free volume at the lower density and the spacer molecules added in the first stage of the construction of the polymer boxes were sufficient for the generation of catenation-free structures.

After the cell construction at the initial density, the models were subjected to sequences of energy minimization and dynamic runs at constant number of particles, temperature and volume (NVT-MD), combined with force field parameter scaling. The cells were then refined by using simulated annealing runs with NVT-MD dynamics: the cells were first heated in three steps from 300 to 800 K. Then the annealed cells were cooled back to 300 K.

The cells were later pressurized to increase their experimental density, at 300 K by using several cycles of simulation runs at constant particle number, temperature and pressure (NPT-MD). The boxes were later put through a stage-wise equilibration procedure by using again simulated annealing runs and cooling back to 300 K with NVT-MD dynamics. Finally the systems were relaxed by NPT dynamics at 1 bar and 300 K

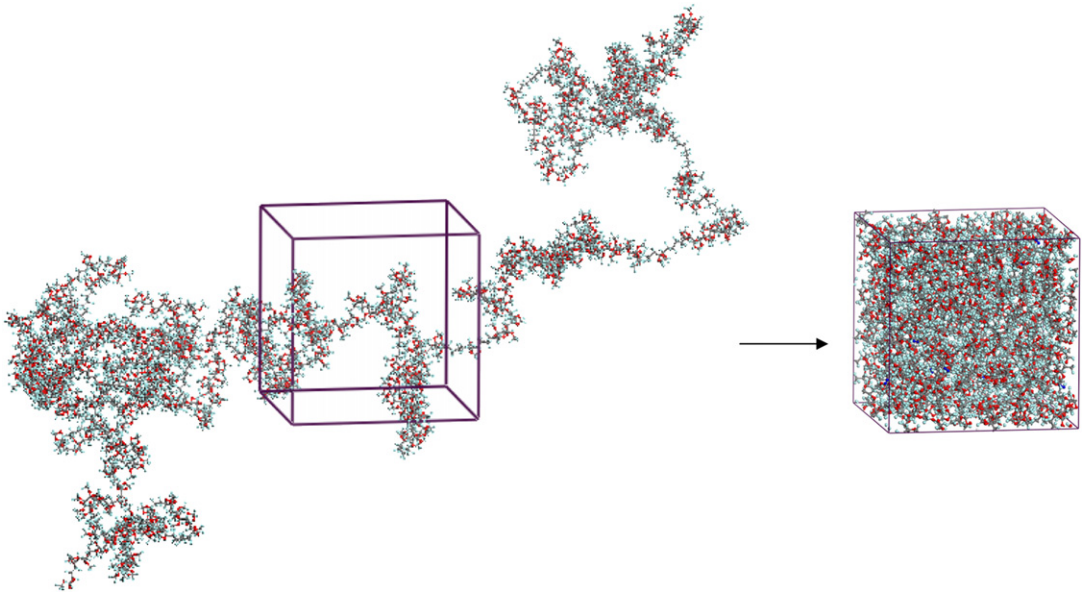

Fig. 4. Construction of a fully equilibrated three-dimensional box, starting with a single Hyflon AD60X polymer chain. Atom colors: grey = carbon, red = oxygen, light blue = fluorine. Ten nitrogen molecules (dark blue) are inserted into the box for the transport studies. (For interpretation of the references to color in this figure legend, the reader is referred to the web version of this article.)

to ensure that a constant density has been reached. Small deviations may happen in obtaining the experimental density for glassy stiff-chain polymer materials [34,35], especially if the models are rather large. The deviations may reflect minor errors of the parameterization of the respective polymers in the chosen force field, which influence the equilibration of the models. This final equilibration step is carried out for 300 ps.

The general simulation conditions used were: minimum image boundary condition to make the system numerically tractable and to avoid symmetry effects; a cut-off distance of 22 Å with a switching function in the interval 20.5–22 Å. During the dynamics the Andersen et al. [36] temperature control and the Berendsen et al. [37] pressure control methods were used. NPT-MD simulations for the further analysis (collection of data) at 1 bar were performed with the Discover Insight II package of Accelrys [30] employing a time step of 1 fs for the numerical integration for 1.2 ns. Positions and velocities of all the atoms of the model structures were saved each 500 ps in a history file. Parallel to the MD simulations the reasonably equilibrated packing models were subjected to the Transition-State Theory algorithm using the GSNET and GSDIF programs [38].

2.9.2. Theoretical calculation of diffusion coefficients

The diffusion coefficients (D) for penetrant molecules were calculated via the long term molecular dynamics (MD) method by means of the Einstein relation [39]:

$$D = \frac{1}{6} N_a \lim_{t\to\infty} \frac{d}{dt} \sum_{i=1}^{N_a} \left\langle |\mathbf{r}_i(t) - \mathbf{r}_i(0)|^2 \right\rangle \tag{14}$$

where N_a is the number of diffusing molecules of type a, $\mathbf{r}_i(0)$ and $\mathbf{r}_i(t)$ are the initial and final positions of molecules (of centres of mass of particle, i) over the time interval t, and $\left\langle |\mathbf{r}_i(t) - \mathbf{r}_i(0)|^2 \right\rangle$ is the mean squared displacement (MSD), averaged over the possible ensemble. The Einstein relation assumes a random walk motion for the diffusing particle. The anomalous diffusion, generally observed for glassy polymers in the range of short times, is characterized by the mean squared displacement [40]:

$$\left\langle |\mathbf{r}_i(t) - \mathbf{r}_i(0)|^2 \right\rangle \propto t^n \tag{15}$$

with $n < 1$. In the short simulation time the MSD may be quadratic due to the fact that the penetrant molecule is restrained in its motion in the rigid structure.

The dissolved gas is assumed to be at infinite dilution. However, in order to enhance the sampling efficiency, 10 molecules of each gas type have been inserted into the polymer structure. For the given boxes this corresponds to a slightly higher nitrogen and oxygen concentration than the experimental solubilities, while the helium concentration is notably higher than the experimental solubility at 1 bar in the melt-pressed membrane. Nevertheless, for the simulations this does not give any complications. The concentrations are still sufficiently low and there are no significant mutual interactions between the dissolved gas molecules. It is also experimentally known that these very low concentrations still have no effect on the polymer matrix. Only highly soluble gases at elevated pressures may cause plasticization, and thus significant modification of the polymer structure. This is for instance the case with CO_2 at pressures higher than 10–20 bar.

2.9.3. Theoretical calculation of diffusion and solubility coefficients with the TST

Transition-State Theory (TST) is used to calculate the rate constants, k_{jump}, of each possible jump from cavity to cavity

in a polymer microstructure and it is used to compute diffusion and solubility coefficients. Gusev and Suter implemented the original TST method giving the polymer some flexibility [41,42] and assuming that the polymer atoms in a sorption site execute uncorrelated harmonic vibrations around their equilibrium positions to accommodate the guest molecules. These motions are termed elastic motions and they occur at a much shorter time scale than the time elapsing between penetrant jumps. The behaviour and properties of the solute can be described with the time-independent single-particle distribution function, $\rho(\vec{\tau})$, where $\vec{\tau}$ is the location [41,42], thus allowing for modelling the transport of small molecules in solids on time scales far beyond the reach of MD. The thermal fluctuations of the position of all the atoms are described by the isotropic Gaussian functional form, using the mean squared deviation of host atoms from their average positions, given by:

$$W(\{\Delta\}) \propto \exp\left\{ -\sum \frac{\Delta^2}{2\langle \Delta^2 \rangle} \right\} \tag{16}$$

The smearing factor $\langle \Delta^2 \rangle$ is a parameter in the homogeneous isotropic approximation and can be evaluated from atomistic trajectories of the polymeric matrix by means of short-scale MD simulations of the host matrix without dissolved molecules. It is assumed that the averaging time for the determination of the smearing factor $\langle \Delta^2 \rangle$ should be the most frequent residence time τ of a probe molecule in the void. Since the value of the average residence time of diffusant molecules in the void depends on the thermal vibrations of the polymer matrix an iterative procedure is used, starting with the rather arbitrary setting $\langle \Delta \rangle = 0.3–0.4$ Å and computing $\rho(\log \tau, \langle \Delta^2 \rangle)$. A new iteration with the new values for $\langle \Delta^2 \rangle$ is used and the function is recalculated until the convergence criterion is fulfilled and the smearing factor does not change the position of the maxima of the probability function.

The behaviour and properties of the small gas molecules are described by a time-independent single-particle distribution function $r(\mathbf{r})$, where $\mathbf{r}$ is the position [27,43,44]. This allows the modelling of the transport of probe gases also in glassy polymers on time scales exceeding the diffusive regime and it requires much less computational time than MD.

The application of TST requires (a) preparation of the host polymeric matrix, determining the positions of all the atoms in the matrix; (b) evaluation of the interactions between the diffusant guest molecule and the host matrix that determine the probability of finding the guest particle at each point of the host matrix; (c) random walk of the diffusant through the matrix.

The TST method was thus used to study the thermodynamics and transport of the small gas molecules, hydrogen, oxygen, nitrogen, methane and carbon dioxide, respectively, in the version of Insight II (400P+) [30]. Diffusion coefficients (D) and gas solubility (S) in the matrix were computed and then the permeability coefficients (P) were calculated as the product of D and S (Eq. (7)). The calculations were carried out in two steps. In the first step the solubility of the respective gas was evaluated. A three-dimensional orthogonal lattice grid with a constant spacing of 0.3 Å was used to estimate the solute distribution function in the matrix by calculating the Helmholtz free energy between the gas molecule inserted at each grid point and all the atoms of the polymer matrix that are subjected to elastic fluctuations. These data were used to identify minimum energetic sites and to determine transition probabilities from site to site, together with the residence time in each site. In the second step a Monte Carlo simulation of gas diffusion by a 'hopping' mechanism was performed, based on the energy as well as the connectivity of available sites and on the transition jump probabilities. In this study, the smearing factor was calculated by means of the self-consistent field (SCF) procedure. The mean squared displacement of all subsets of atoms in the amorphous cell was obtained as a function of time from a short NVT dynamics run (30 ps with 1 fs time step at 300 K).

3. Results and discussion

3.1. Quantitative analysis of the residual solvent

Membranes were prepared by a standard solution-casting procedure, followed by evaporation of the solvent at room temperature, first at atmospheric pressure until a solid dense film was obtained, and then under vacuum. Subsequently the amount of residual solvent in the membranes was monitored by periodically weighing the film while it is slowly heated under vacuum. Fig. 5a shows the weight loss as a function of the drying temperature for two membranes cast from different solutions. The membrane with Galden HT 55 contains more solvent after drying at room temperature and reaches constant weight at a higher drying temperatures than the membrane with HFE 7100. Evidently, complete removal of Galden is more difficult due to its higher molar mass: 350 g/mol, compared to 250 g/mol for HFE. In both cases the complete evaporation of the solvent within reasonable time is achieved at temperatures well above 130 °C, the T_g of the polymer, measured as the half-c_p value (see below). Only the increased polymer chain mobility in the rubbery state enables a sufficiently fast diffusion of the solvent, while solvent removal from the glassy state seems to be particularly difficult. It was previously found that thin Hyflon AD60X membranes may retain up to about 3% of solvent even after 3 years at room temperature [17].

3.2. Density

The density of the solvent-free melt-pressed membrane was determined by the buoyancy method, as described in Section 2, using toluene as the non-absorbing liquid. At 20 °C the average density determined by three measurements was 1.917 ± 0.012 g/cm^3, in good agreement with the value of 1.93 reported in the literature [6].

3.3. Influence of the residual solvent on the thermal properties

Differential Scanning Calorimetric (DSC) analysis of the samples shows a strong increase of the T_g with increasing

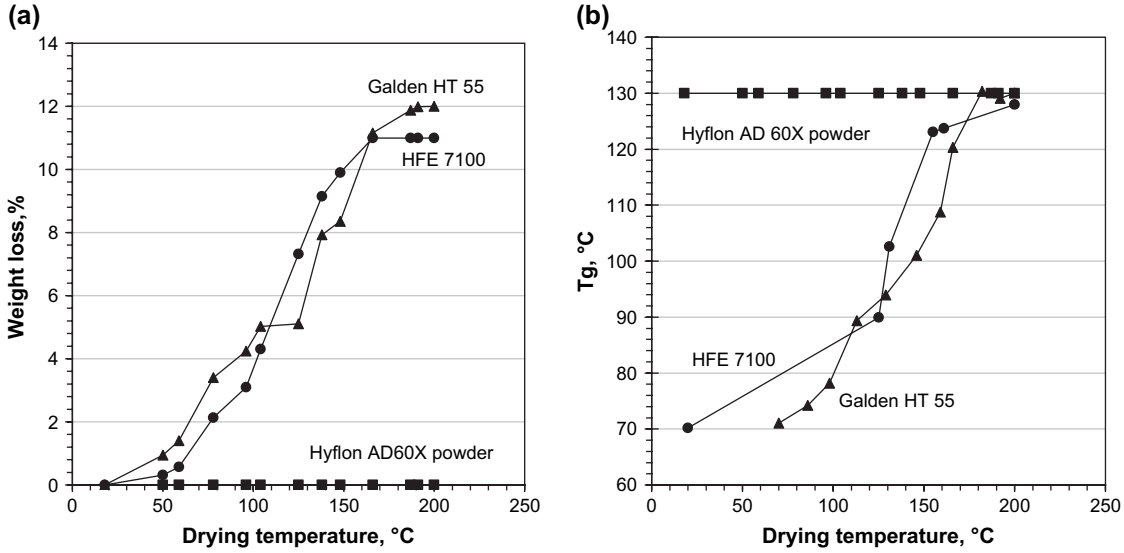

Fig. 5. (a) Weight loss and (b) glass transition temperature of the Hyflon AD60X membranes and of Hyflon powder as a function of the drying temperatures during very slow heating at 0.02 °C/min under vacuum. T_g was determined by DSC from the first heating run at a heating rate of 15 °C/min.

drying temperature and decreasing solvent content (Fig. 5b). Near 200 °C the T_g reaches the same value as the starting polymer powder, which itself does not show any weight loss or change of the T_g over the entire range of drying temperatures. Evidently the residual solvent strongly plasticizes the polymer, reducing the T_g of the freshly cast films to more than 50 °C below that of the pure polymer. Although the trend is clear, the data in Fig. 5b are somewhat scattered. This is because the effect of residual solvent must necessarily be evaluated on the first heating run, which is usually more noisy due to stress relaxation above the T_g and to further evaporation of residual solvent. The second heating curve usually shows a more smooth curve but gives a higher T_g because of partial evaporation of the residual solvent in the first heating/cooling cycle (Fig. 6). The relation between the heating temperature and the T_g (Fig. 5b) is determined both by the amount of the solvent, related to the evaporation rate, and by the relative effect of the solvent on the T_g, related to molecular properties. In the present case both solvents seem to affect the T_g in a similar way.

In quantitative terms the plasticizing effect of HFE and Galden can be evaluated better if the T_g is plotted against the weight fraction of solvent in the film (Fig. 7). Many different equations have been proposed to describe the glass transition temperature of miscible binary polymer blends or polymer/diluent mixtures [45]. One of the most popular relations describing the T_g as a function of the blend composition is the Kwei equation, which is particularly valid for systems with strong interactions between the constituents of the blend [46–48]:

$$T_g = \frac{w_1 T_{g_1} + k w_2 T_{g_2}}{w_1 + k w_2} + q w_1 w_2 \tag{17}$$

in which w_1 is the weight fraction of the first component with glass transition temperature T_{g_1} and w_2 is the weight fraction of the second component with glass transition temperature T_{g_2}; k and q are two adjustable empirical parameters, related to the excess energy of backbone stabilization and to incipient phase inversion [48]. Ruiz-Treviño and Paul, successfully used the Gordon–Tailor equation in their work on membranes with low molecular weight diluents [49–51]. This is a somewhat simplified form of the Kwei equation, with just one adjustable parameter.

$$T_g = \frac{w_d T_{gd} + k w_p T_{gp}}{w_d + k w_p} \tag{18}$$

in which d and p represent the diluent and the polymer, respectively. Probably the most frequently used and simplest relation, without adjustable parameters, is the Fox equation, which will be evaluated in the present work [52]:

$$\frac{1}{T_g} = \frac{w_1}{T_{g_1}} + \frac{w_2}{T_{g_2}} \tag{19}$$

Due to the reciprocal terms, the T_g of the mixture according to the Fox equation is always below the weighted average of the two individual T_gs. If we choose the index 1 for the polymer and 2 for the solvent, then after substitution of $w_1 = 1 - w_2$ the Fox equation can be rewritten in a linearized form:

$$\frac{1}{T_g} - \frac{1}{T_{g_1}} = w_2 \left(\frac{1}{T_{g_2}} - \frac{1}{T_{g_1}} \right) \tag{20}$$

A plot of $(1/T_g) - (1/T_{g_1})$ against the weight fraction of the solvent, w_2, should thus yield a straight line through the origin, with slope $(1/T_{g_2}) - (1/T_{g_1})$. If the T_g of the solvent is not known, then it can be estimated by a linear least squares fit of the experimental data according to Eq. (20) or it can be obtained directly by a nonlinear fit according to Eq. (19). On the other hand, if both T_{g_1} and T_{g_2} are known, then the

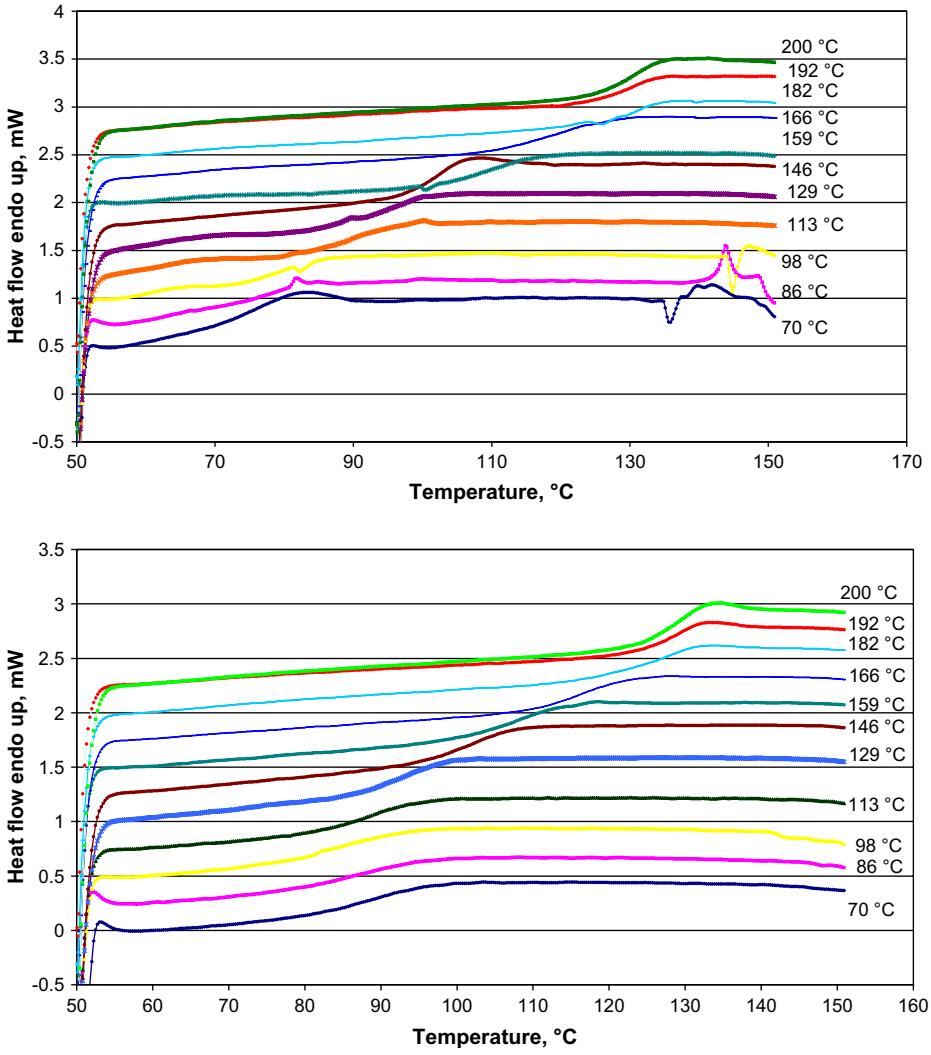

Fig. 6. DSC curves of the membrane prepared from a solution in Galden HT 55, after heating the sample under vacuum to the indicated temperature at 0.02 °C/min. First heating run (top) and second heating run (bottom) at 15 °C/min. Curves are shifted vertically for clarity. The temperatures at the right of the curves indicate the maximum annealing temperature used to remove the solvent.

Fox equation allows the determination of the solvent content by measurement of the T_g.

The experimental values of T_g as a function of the residual solvent content are plotted in Fig. 7. The dotted lines represent the nonlinear fit of the Fox equation, resolving for the unknown value of T_{g_2}, using the experimental weight fractions of solvent and $T_{g_1} = 130$ °C for pure Hyflon AD60X. Thus the estimated values of the T_g of HFE is −120 °C and that of Galden HT 55 is −80 °C. The latter is somewhat overestimated, because its actual T_g is below −100 °C [53] and indicates that the Fox equation fits reasonably well but not perfectly with the experimental data. Nevertheless below 10–15% of residual solvent this fit provides a reasonable estimation of the solvent content if the T_g of an unknown sample is measured. At the same concentration HFE appears to plasticize Hyflon slightly more than Galden HT, probably because of the $-CF_3$ side groups (Scheme 1), which reduce the chain mobility of Galden. Nevertheless, HFE may be more suitable for preparation of dense membranes because of its easier removal.

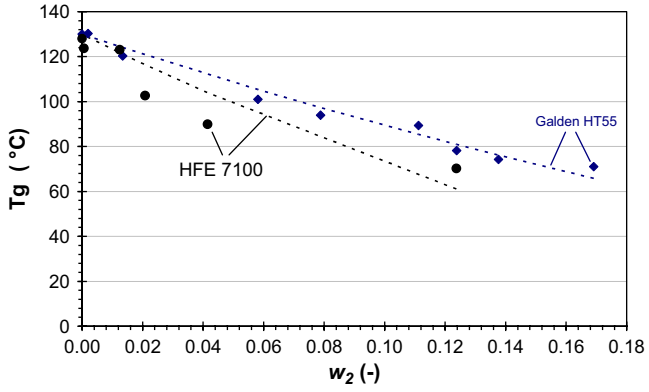

Fig. 7. Glass transition temperatures as a function of the weight fraction of the solvent in the dense film for Galden HT 55 (♦) and HFE 7100 (●). Dotted lines: nonlinear regression curve of the Fox equation (Eq. (19)), solving for the unknown value of T_{g_2} for Galden and for HFE 7100.

Table 2
Mechanical properties of the solvent-cast film before and after drying at 200 °C under vacuum[a]

		Average	Standard deviation	Variance
Fresh film	Young's modulus (MPa)	761	32	4.2
	Maximum load (MPa)	8.82	1.22	13.8
	Elongation at break (%)	1.46	0.31	21.3
Dried film	Young's modulus (MPa)	323	42	13
	Maximum load (MPa)	2.43	0.53	21.8
	Elongation at break (%)	0.85	0.16	18.9

[a] Average of four samples.

3.4. Influence of the solvent on the mechanical properties

The mechanical properties of a freshly prepared film and a vacuum-dried film are listed in Table 2. Remarkably, both the Young's modulus, the maximum elongation and maximum strength, decrease as a result of the drying procedure. Especially the lower Young's modulus seems to be in contradiction with the strong plasticization found by DSC analysis. Paul and coworkers observed a similar effect in a series of membranes with different low molar mass diluents, defining the phenomenon as antiplasticization [50,51,54–57]. They further observed that the increase in strength was accompanied by a decrease of the free volume. For this reason their diluent molecules caused a decrease in the gas permeability and an increase in the selectivity, in sharp contrast with the observations in this paper (see transport properties below). In the present work it was furthermore observed that drying at elevated temperature is usually accompanied by a contraction of the sample specimen of up to about 20% of its original diameter, and by a slight increase of the film thickness. The predominance of contraction in the in-plane direction suggests that in the last stage of the solvent evaporation process the chains have undergone a net orientation as a result of the unidirectional diffusion of the solvent to the membrane surface (Fig. 8). This orientation then relaxes upon heating the sample above the T_g, resulting in the observed contraction.

We can thus attribute the observed results to two distinct phenomena. The first, true plasticization by the residual solvent dominates the thermal properties and the gas transport. The second, the introduction of anisotropy in the polymer sample by the solvent evaporation dominates the mechanical properties.

3.5. Influence of residual solvent on gas permeation

In order to quantify the effect of the residual solvent on the transport properties, permeation measurements were carried out on membranes cast from solutions in HFE as well as Galden, before and after thorough removal of the residual solvent under vacuum. A melt-pressed membrane, prepared in the complete absence of solvent, was investigated for comparison. The automated gas permeation setup (Fig. 1) has such a rapid response that it enables accurate measurements of the time lag of very fast gases such as helium and hydrogen. An example of the experimental time-lag curves of membrane H25 is given in Fig. 9. The time lag is obtained by extrapolation of the steady state pressure increase curve to the starting pressure while the diffusion coefficients of the gases in the polymer are calculated from the time lag according to Eq. (12). The permeability and solubility are then obtained from the steady state pressure increase rate, as described above. An overview of all experimental data of the different membranes is given in Tables 3 and 4.

3.5.1. Gas diffusion measurements

The diffusion coefficient strongly decreases with increasing molecular size of the gas, indicating a considerable size-sieving character of Hyflon AD60X (Fig. 10). Furthermore, depending on the specific gas species, the diffusion coefficient may change dramatically upon drying of the membrane. Diffusion in the freshly cast membrane is generally much faster than in the solvent-free membrane, in particular for the gases with a large kinetic diameter, such as CO_2 and methane. As discussed above on the basis of the thermal properties, this is due to plasticization of the polymer by the residual solvent, which favours especially the motion of the bulkier molecules. Both the polymer and the solvent are highly hydrophobic and lack the molecular interactions which are responsible for the antiplasticization observed by Paul and coworkers [50,51,54–57]. The membranes prepared from HFE and from Galden demonstrate similar behaviour, although the latter has initially a higher permeability and a lower selectivity due to a slightly higher residual solvent content. After complete removal of the solvent under vacuum the solution-cast membranes have nearly the same properties

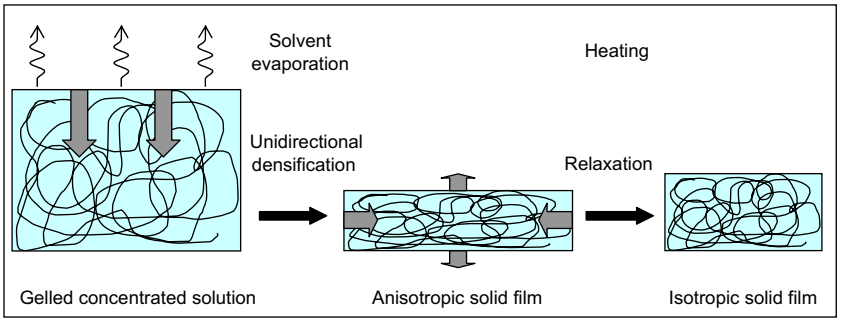

Fig. 8. Schematic representation of the orientation and relaxation phenomena of the polymer during solvent evaporation from the film below and above the T_g, respectively.

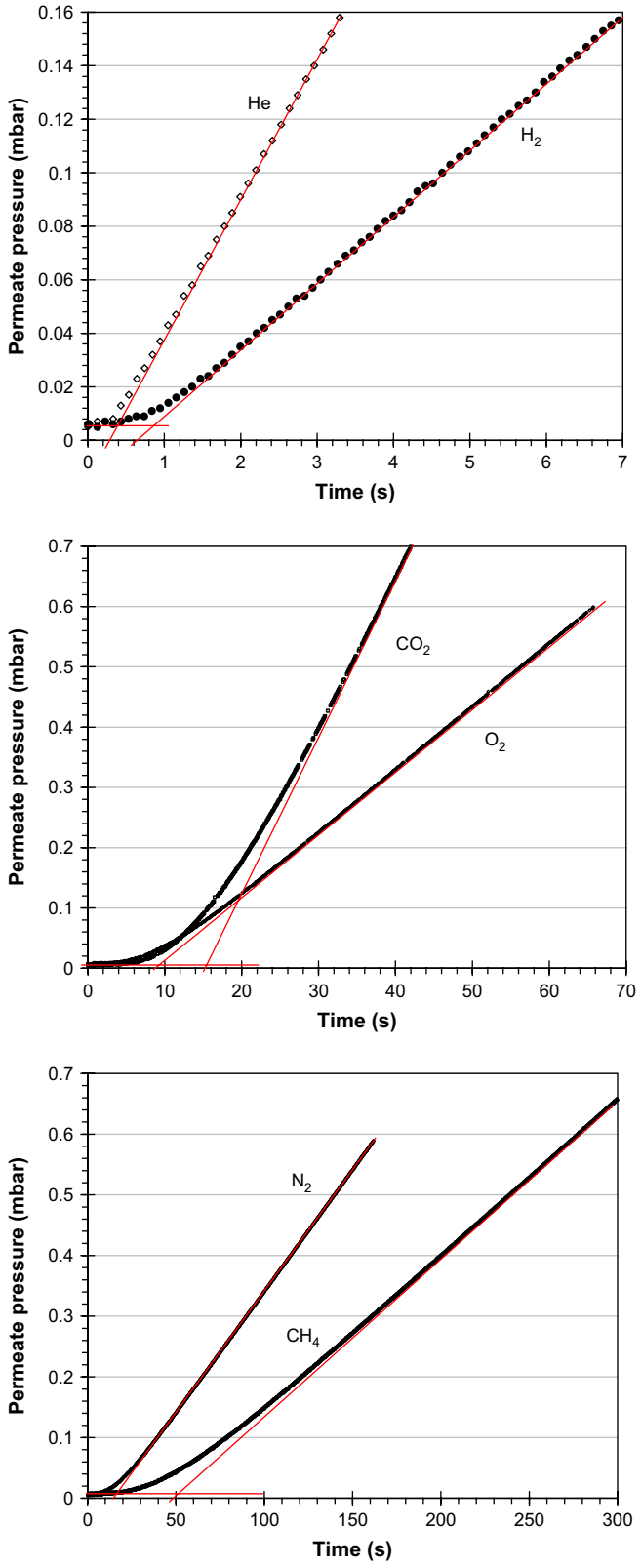

Fig. 9. Pressure increase curves of the freshly cast membrane H25 for six different gases at 25 °C and at a feed pressure of 1 bar. Membrane area 11.3 cm^2; permeate volume 75.5 cm^3.

as the melt-pressed sample. Since both types of membrane have been treated above the T_g, the sample history is cancelled and becomes irrelevant, in contrast to what can be observed if the solvent is removed below the T_g [18]. The increase in permselectivity of the membranes upon removal of the residual solvent can be ascribed entirely to the increase of diffusion selectivity. In the absence of residual solvent the Hyflon membranes have a CO_2/CH_4 selectivity of about 25. Although this is not exceptionally high, the combination with a relatively high CO_2 permeability and an excellent resistance to swelling by condensable species such as higher hydrocarbons, make this material nevertheless attractive for natural gas treatment.

3.5.2. Gas diffusion simulations

The theoretical diffusion coefficients were also obtained from simulations by using the TST method and by MD runs at 300 K. The data obtained by TST studies are plotted together with the experimental data in Figs. 10 and 11. They follow the same trend as the experimental results, although the absolute values of all diffusion coefficients obtained by TST are about one order of magnitude higher. The discrepancy between the experimental and theoretical data may have several reasons. The first is related to the construction of the model, where small deviations may occur in the density. This happens especially for glassy stiff-chain polymer materials [34,35] and when the model is rather large. These deviations may reflect minor errors of the parameterization of the respective polymers in the chosen force field, which influence the equilibration of the models. The second is related to assumptions about the diffusing species and the polymer. It must be emphasized that the TST calculations assume that the penetrant molecules are spherical united atoms, defined by effective Lennard–Jones parameters, σ (Å) and ε (kcal/mol). It is furthermore assumed that the polymer packing does not undergo structural relaxation (e.g. resulting from torsion transitions) to accommodate an inserted particle. Therefore, this simulation technique is restricted to small molecules. The large deviations for CO_2 and CH_4 may be explained by their relatively large dimensions, necessitating a certain dilation of the polymer matrix for their insertion. An additional reason for the deviation of CO_2 may be the well known experimental fact of plasticization of the glassy membrane due to specific interactions of CO_2 with the polymer matrix, leading to membrane structural relaxations. This behaviour "violates" the assumption of the TST in which the dynamics of the dissolved molecules is coupled only to the elastic thermal motion of the dense polymer. The results for CO_2 clearly show the necessity to develop improved TST methods which permit the matrix to be locally flexible in order to accommodate larger penetrant molecules that are described in all-atom representation with partial charges. A better agreement between simulated and experimental D and S for N_2 and O_2 would require a re-parametrization of the Lennard–Jones parameters of both gas molecules, and improvement of the force field for the polymer, but this is beyond the scope of the present study.

The gas diffusion was further calculated using Eq. (14) from the MSD over the range of simulation times from 0.5

Table 3
Experimental transport parameters at 25 °C and 1 bar of feed gas pressure for solution-cast membranes from casting solutions in Galden HT 55 or HFE 7100 before and after vacuum drying at 200 °C

Membrane	Gas	Permeability coefficient, P		Time lag, Θ (s)	Diffusion coefficient, D (10^{-6} cm^2/s)	Solubility, S (m^3_{STP}/m^3 bar)	Selectivity		
		10^{-6} m^3_{STP} m/(m^2 h bar)	Barrer[a]				P_i/P_{N_2} (−)	D_i/D_{N_2} (−)	S_i/S_{N_2} (−)
Membrane G25; solvent Galden; freshly cast; thickness 60.6 μm	Helium	0.976	357	0.21	29.1	0.093	9.37	37.62	0.249
	Hydrogen	0.515	188	0.41	14.9	0.0958	4.94	19.27	0.256
	CO_2	0.576	210	7.5	0.816	1.96	5.52	1.05	5.24
	Oxygen	0.232	84.7	4.6	1.33	0.484	2.22	1.72	1.30
	Nitrogen	0.104	38.1	7.9	0.775	0.374	1.00	1.00	1.00
	Methane	0.0844	30.8	15.5	0.395	0.593	0.81	0.51	1.59
Membrane G200; solvent Galden; dried at 200 °C; thickness 65.2 μm	Helium	1.3	476	0.23	30.8	0.117	50.3	187.0	0.269
	Hydrogen	0.511	187	0.7	10.1	0.140	19.72	61.4	0.321
	CO_2	0.211	77.0	35	0.202	2.89	8.14	1.23	6.62
	Oxygen	0.0948	34.6	17	0.417	0.632	3.66	2.53	1.45
	Nitrogen	0.0259	9.46	43	0.165	0.436	1.00	1.00	1.00
	Methane	0.00828	3.03	290	0.0244	0.941	0.32	0.15	2.16
Membrane H25; solvent HFE 7100; freshly cast; thickness 67.7 μm	Helium	0.928	339	0.29	26.3	0.0978	12.93	53.5	0.242
	Hydrogen	0.461	169	0.51	15.0	0.0856	6.43	30.4	0.212
	CO_2	0.455	166	11.8	0.647	1.95	6.34	1.31	4.83
	Oxygen	0.189	69.1	7.4	1.03	0.509	2.63	2.09	1.26
	Nitrogen	0.0718	26.2	15.5	0.493	0.404	1.00	1.00	1.00
	Methane	0.0549	20.1	66	0.116	1.32	0.77	0.23	3.26
Membrane H200; solvent HFE 7100; dried at 200 °C; thickness 68.3 μm	Helium	1.24	455	0.3	26.3	0.131	41.0	126.7	0.323
	Hydrogen	0.509	186	0.62	12.7	0.111	16.8	61.3	0.273
	CO_2	0.220	80.3	37	0.214	2.86	7.24	1.03	7.05
	Oxygen	0.106	38.7	15	0.527	0.559	3.49	2.53	1.38
	Nitrogen	0.0304	11.1	38	0.208	0.406	1.00	1.00	1.00
	Methane	0.00916	3.35	260	0.0304	0.837	0.30	0.15	2.06

[a] 1 barrer = 10^{-10} cm^3_{STP} cm/(cm^2 s cmHg).

to 1.2 ns where Einstein diffusion is observed. The results are indicated in Fig. 10 and clearly show a better agreement with the experimental data than the values obtained with the TST method. The difficulties for MD simulations in glassy polymers lie in the extremely broad distribution of gas molecule jump rates. It is known that the diffusion of a penetrant in a glassy polymer involves occasional jumps between cavities through the opening of a channel [34,35]. Jumps are rare

Table 4
Experimental transport properties at 25 °C and 1 bar of feed gas pressure for a melt-pressed membrane prepared at 170 °C, and transport properties at 25 °C obtained by TST and MD simulations

Membrane	Gas	Permeability coefficient, P		Time lag, Θ (s)	Diffusion coefficient, D (10^{-6} cm^2/s)	Solubility, S (m^3_{STP}/m^3 bar)	Selectivity		
		10^{-6} m^3_{STP} m/(m^2 h bar)	Barrer[a]				P_i/P_{N_2} (−)	D_i/D_{N_2} (−)	S_i/S_{N_2} (−)
Membrane M170 [17]; melt-pressed at 170 °C; thickness 220 μm	Helium	1.11	405	1.57	51.4	0.0599	48.9	385.4	0.127
	Hydrogen	0.382	140	6.2	0.130	0.0815	16.9	97.6	0.173
	CO_2	0.173	63.3	400	0.202	2.39	7.65	1.51	5.06
	Oxygen	0.0786	28.7	185	0.436	0.501	3.47	3.27	1.06
	Nitrogen	0.0226	8.27	605	0.133	0.472	1.00	1.00	1.00
	Methane	0.00664	2.43	2710	0.0297	0.620	0.29	0.22	1.32
Pure Hyflon AD60X; TST simulations	Helium								
	Hydrogen	19.3	7.13×10^3		103	0.527	3.38	12.6	0.269
	CO_2	33.8	1.25×10^4		2.13	44.7	5.94	0.260	22.8
	Oxygen	15.5	5.74×10^3		14.3	3.05	2.72	1.75	1.55
	Nitrogen	5.7	2.11×10^3		8.18	1.96	1.00	1.00	1.00
	Methane	15.9	5.90×10^3		5.66	7.93	2.80	0.69	4.04
Pure Hyflon AD60X; MD simulations	Helium				76.8			175.3	
	Hydrogen								
	CO_2								
	Oxygen				0.401			0.916	
	Nitrogen				0.438			1.00	
	Methane								

[a] 1 barrer = 10^{-10} cm^3_{STP} cm/(cm^2 s cmHg).

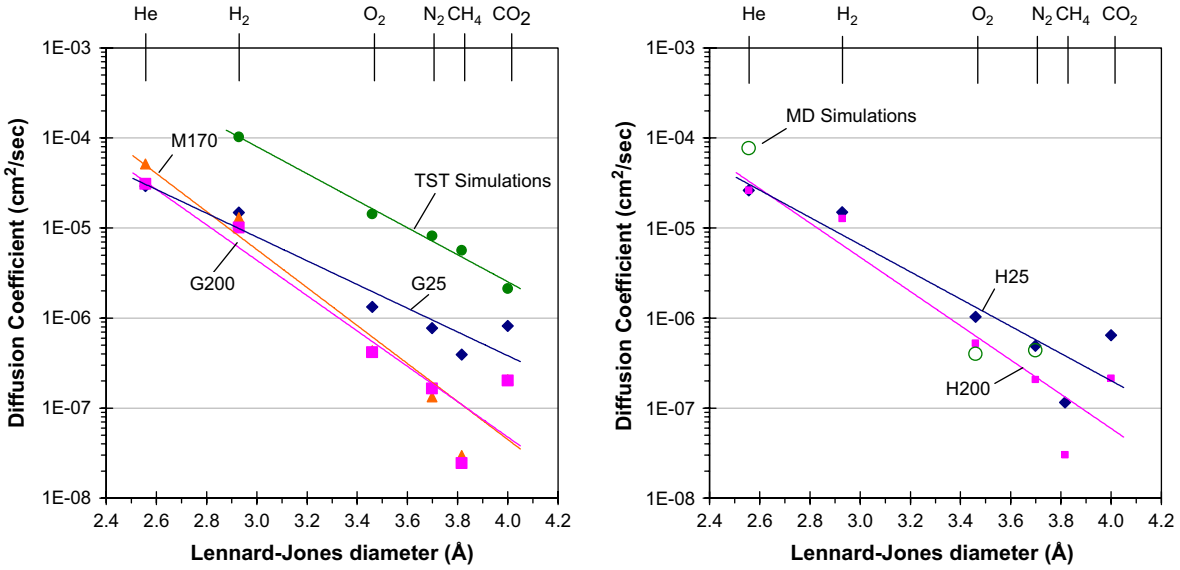

Fig. 10. Diffusion coefficients of six gases in a solution-cast membrane, obtained with Galden HT 55 (left) and HFE 7100 (right) before (♦) and after (■) drying under vacuum. Comparison with a melt-pressed membrane, M170 (▲), and with theoretical data from TST (●) and from MD simulations (○).

events and the time between them is often shorter than the times governing matrix relaxation processes. In spite of these limitations, MD simulations are a very powerful technique and preliminary calculations on oxygen, nitrogen and helium molecules were therefore carried out in the present work. Since the quality of MD results strongly depends on the box construction, studies are currently in progress to improve the box construction and to make MD calculations more feasible, so that a better correlation between the experimental and the theoretical results can be achieved.

3.5.3. Gas solubility measurements

The penetrant solubility of all gases in the different membranes is calculated from the corresponding diffusion constant and the steady state permeability according to Eq. (7) and is listed in Tables 3 and 4. It tends to increase with increasing condensability (i.e. higher critical temperature or higher normal boiling point) of the gas and in the presence of more favourable interactions with the polymer. Often a linear trend is observed between the logarithm of the solubility and the critical temperature of the absorbed gas [58]. The present results indeed show a clear correlation between solubility and critical temperature (Fig. 11). Unlike the diffusion coefficient, the solubility hardly changes in the presence or absence of residual solvent. This is because the solubility is mainly related to the interactions between the penetrant and the polymer matrix. Since the solvent has similar physical–chemical properties as the polymer, its presence has little effect on the gas solubility. The differences between the membranes prepared from the two solvents, either before or after vacuum drying,

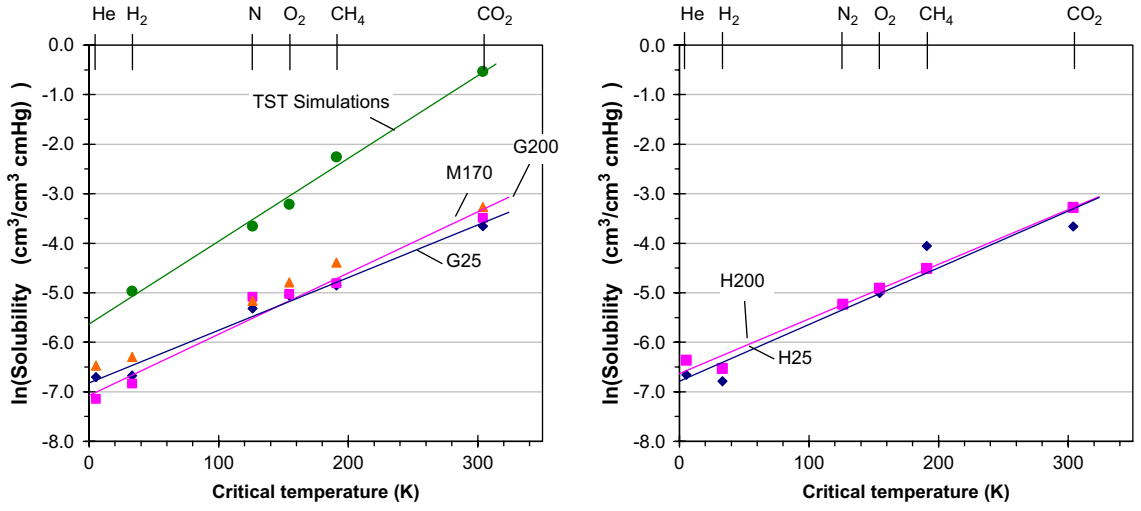

Fig. 11. Solubility coefficients of six gases in a solution-cast membrane, obtained with Galden HT 55 (left) and HFE 7100 (right) before (♦) and after (■) drying under vacuum. Comparison with a melt-pressed membrane, M170 (▲) and with theoretical data from TST simulations (●).

are within the range of the experimental error. Furthermore, the gas solubilities in the solution-cast membranes are nearly identical to those of the melt-pressed sample. It is evident that the sample history has a much stronger effect on the diffusion than on the gas solubility.

3.5.4. Gas solubility simulations

The simulated solubility values are substantially higher than the experimental data (Fig. 11 and Table 4). This is to some extent due to the thermodynamic non-equilibrium state of glassy polymers, which modifies the polymer–penetrant interactions and thus provokes relatively high deviations of simulated and experimental solubility coefficients. An additional reason could be related to the packing procedure and to the available data for the modelling: even relatively small errors in the insertion energy, which are determined by the quality of the model and of the applied force fields, may lead to rather high deviation in the simulated solubilities [59]. For these reasons developments to obtain new or improved models are in continuous evolution [60].

From Sections 3.3 to 3.5 it follows that the direct and indirect effects of the solvent on the membrane performance are many and that they can roughly be arranged under two distinct phenomena:

(A) True plasticization by the residual solvent dominates the thermal properties and the gas transport properties, reducing both the T_g and the permselectivity.
(B) The anisotropy of the sample, induced by the solvent evaporation, dominates the mechanical properties, increasing the Young's modulus and the tensile strength of the sample.

From the present results it is impossible to establish independently in which way the anisotropy influences the transport properties.

In this light the results of Yampolskii et al. are particularly interesting [26,61]. They observed that thorough drying under strain causes an even stronger increase in the selectivity than the solvent removal in the present work. Their so-called 'strained aging' in conditions where the polymer is not allowed to relax [24,25] also suggests the introduction of a certain anisotropy in the sample. However, they explained the results entirely in terms of conformational changes in the polymer chain and did not perform mechanical or other tests that could witness macroscopic anisotropy in the aged membranes.

3.6. Solid-state NMR spectroscopy

The ^{1}H HRMAS NMR spectra in Fig. 12 of the solution-cast membrane, dried at different temperatures, give clear evidence of the presence of the solvent HFE and show a qualitative picture of the progress of the solvent removal. The spectrum of the freshly prepared membrane shows two major peaks. The most intense line is attributed to the methoxy group of HFE. Its intensity decreases with the drying temperature and the peak disappears at 200 °C, evidencing the complete removal of the solvent. The few small peaks, centred around a less intense second line can be attributed to the presence of protonated impurities in Hyflon, and in particular to traces of the initiator or of the surfactants used during the polymerization [53].

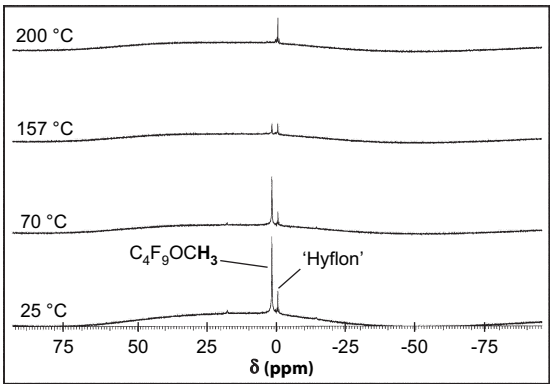

Fig. 12. HRMAS ^{1}H NMR spectra of a Hyflon film after drying at room temperature at atmospheric pressure and of three films after drying under vacuum at the indicated temperatures (vertical scales not normalized).

Besides this qualitative information on the amount of solvent, the NMR spectra give important extra information about the state of the solvent. The single sharp solvent peak indicates that only one kind of solvent exists in the polymer matrix, i.e. either bound or unbound, or that the dynamics of the transition between the bound and the unbound state of the solvent molecules is faster than the time scale of the NMR analysis. The latter hypothesis can be excluded by the fact that no change in the chemical shift of the methoxy peak occurs at different solvent concentrations. If the solvent were present in two different states with a very fast interchange, then the average chemical shift would be expected to depend on the relative amount of the two states and, most likely, on the total amount of solvent present. NMR analysis thus seems to confirm that the origin of the particular solvent retention by the Hyflon membranes must not be found in special interactions between solvent and polymer matrix but only in the kinetics of the solvent diffusion. This is reasonable, considering the very high molar mass of the solvent molecules. Extrapolation of the curves in Fig. 10 to much higher Lennard–Jones diameter indeed suggests that the diffusion of the solvents is several orders of magnitude slower than that of the permanent gases studied in this paper.

4. Conclusions

Hyflon AD60X is a perfluorinated polymer with a relatively high gas permeability due to its high fractional free volume. It was found that the solvents used for solution-casting of dense membranes tend to be retained much more in the polymer matrix than expected for a similar high free volume polymer. In this paper the effect of the residual solvent on the thermal, mechanical and transport properties of solution-cast membranes has been studied. Thermal analysis reveals that residual solvent plasticizes the polymer and strongly affects its gas transport properties, increasing noticeably the diffusion coefficient

of the gases with a high molecular size and reducing the membrane's permselectivity. Complete removal of the solvent from thick films within reasonable time requires treatment under vacuum far above the T_g. This treatment noticeably increases the selectivity compared to freshly cast membranes. Comparison of the data of vacuum-dried solvent-free membranes with a melt-pressed sample gives nearly the same results. The potential presence of residual solvent in solution-cast membranes prepared under mild conditions should always be taken into account in practical applications or when interpreting experimental data.

The possible cause of the unexpectedly high solvent retention was studied by solid-state NMR analysis of samples with different concentrations of residual solvent. Detailed analysis did not show any evidence of specific interactions between the entrapped solvent and the polymer matrix. This is an indication that the solvent retention is kinetically determined rather than thermodynamically, i.e. it is a result of slow diffusion of the solvent molecules through the polymer matrix. The solvent retention in Hyflon might further be related to the absence of strong cohesive forces in the polymer and the consequently high fractional free volume.

Simulation studies according to the transition-state theory reproduce the trend in the experimental solubility and diffusion coefficients as a function of the critical temperature and the molecular dimensions, respectively. Nevertheless, the absolute values are in both cases sensibly higher in the simulations than those measured experimentally. This is probably due to imperfections in the force field and to the strong dependence of the data on the box equilibration. MD simulations reproduce the experimental data better but require much more computational effort. Improvement of the computational methods is necessary and is subject of further studies.

Acknowledgements

The work was financed by the European Commission 6th Framework Program Project MultiMatDesign "Computer aided molecular design of multifunctional materials with controlled permeability properties Contract Number: NMP3-CT-2005-013644". Solvay-Solexis is gratefully acknowledged for providing Hyflon AD60X and Galden HT 55.

References

[1] Alentiev AYu, Yampolskii YuP, Shantarovich VP, Nemser SM, Platé NA. High transport parameters and free volume of perfluorodioxole copolymers. J Membr Sci 1997;126:123–32.

[2] Merkel TC, Pinnau I, Prabhakar R, Freeman BD. Gas and vapor transport properties of perfluoropolymers. In: Yampolskii Yu, Pinnau I, Freeman BD, editors. Materials science of membranes for gas and vapor separation. Chichester, England: John Wiley & Sons; 2006 [chapter 9].

[3] Pinnau I, Toy LG. Gas and vapor transport properties of amorphous perfluorinated copolymer membranes based on 2,2-bistrifluormethyl-4,5 difluoro-1,3 dioxole/tetrafluoroethylene. J Membr Sci 1996;109:125–33.

[4] Merkel TC, Bondar V, Nagai K, Freeman BD. Hydrocarbon and perfluorocarbon gas sorption in poly(dimethylsiloxane), poly(1-trimethylsilyl-1-propyne), and copolymers of tetrafluoroethylene and 2,2-bis(trifluoromethyl)-4,5-difluoro-1,3-dioxole. Macromolecules 1999;32:370–4.

[5] Arcella V, Colaianna P, Maccone P, Sanguineti A, Gordano A, Clarizia G, et al. A study on a perfluoropolymer purification and its application to membrane formation. J Membr Sci 1999;163:203–9.

[6] Pinnau I, He Z, Da Costa AR, Amo KD, Daniels R. Gas separation using organic-vapor-resistant membranes. US Patent 6,361,583; 1992.

[7] Prabhakar RS, Freeman BD, Roman I. Gas and vapor sorption and permeation in poly(2,2,4-trifluoromethoxy-1,3-dioxole-*co*-tetrafluoroethylene). Macromolecules 2004;37:7688–97.

[8] Park JY, Paul DR. Correlation and prediction of gas permeability in glassy polymer membrane materials via a modified free volume based group contribution method. J Membr Sci 1997;125:23–39.

[9] Golemme G, Nagy JB, Fonseca A, Algieri C, Yampolskii Yu. ^{129}Xe NMR study of free volume in amorphous perfluorinated polymers: comparison with other methods. Polymer 2003;44:5039–45.

[10] Pinnau I, He Z, Da Costa AR, Amo KD, Daniels R. Gas separation using C_{3+} hydrocarbon-resistant membranes. US Patent 6,361,582; 1992.

[11] Jansen JC, Tasselli F, Tocci E, Drioli E. High-flux composite perfluorinated gas separation membranes of Hyflon® AD on a hollow fibre ultrafiltration membrane support. Desalination 2006;192:207–13.

[12] Petropoulos JH. Plasticization effects on the gas permeability and permselectivity of polymer membranes. J Membr Sci 1992;75:47–59.

[13] White LS, Blinka TA, Kloczewski HA, Wang I-F. Properties of a polyimide gas separation membrane in natural gas streams. J Membr Sci 1995;103:73–82.

[14] Wind JD, Paul DR, Koros WJ. Natural gas permeation in polyimide membranes. J Membr Sci 2004;228:227–36.

[15] Polyakov AM, Starannikova LE, Yampolskii YuP. Amorphous Teflons AF as organophilic pervaporation materials: transport of individual components. J Membr Sci 2003;216:241–56.

[16] Polyakov AM, Starannikova LE, Yampolskii YuP. Amorphous Teflons AF as organophilic pervaporation materials: separation of mixtures of chloromethanes. J Membr Sci 2004;238:21–32.

[17] Jansen JC, Macchione M, Drioli E. On the unusual solvent retention and the effect on the gas transport in perfluorinated Hyflon AD® membranes. J Membr Sci 2007;287:132–7.

[18] Joly C, Le Cerf D, Chappey C, Langevin D, Muller G. Residual solvent effect on the permeation properties of fluorinated polyimide films. Sep Purif Technol 1999;16:47–54.

[19] Hacarlioglu P, Toppare L, Yilmaz L. Effect of preparation parameters on performance of dense homogeneous polycarbonate gas separation membranes. J Appl Polym Sci 2003;90:776–85.

[20] Maeda Y. Homogeneous multicomponent glassy polymers as membranes for gas separations. PhD thesis, The University of Texas at Austin; 1985.

[21] Nemser SM, Roman IC. Perfluorinated membranes. US Patent 5,051,114; 1991.

[22] Khulbe KC, Matsuura T, Lamarche G, Kim HJ. The morphology characterisation and performance of dense PPO membranes for gas separation. J Membr Sci 1977;135:211–23.

[23] Bi J, Simon GP, Yamasaki A, Wang CL, Kobayashi Y, Griesser HJ. Effects of solvent in the casting of poly(1-trimethylsilyl-1-propyne) membranes. Radiat Phys Chem 2000;58:563–6.

[24] Kostina Yu, Bondarenko G, Alentiev A, Yampolskii Yu. The influence of conformation composition of polyheteroarylenes on their transport properties. Desalination 2006;200:34–6.

[25] Alentiev A, Yampolskii Y, Kostina Yu, Bondarenko G. New possibilities for increasing the selectivity of polymer gas separating membranes. Desalination 2006;199:121–3.

[26] Kostina Yu, Bondarenko G, Alentiev A, Yampolskii Yu. Effect of chloroform on the structure and gas-separation properties of poly(ether imides). Polym Sci Ser A 2006;48:32–8.

[27] Gusev AA, Mueller-Plathe F, van Gunsteren WF, Suter UW. Dynamics of small molecules in bulk polymers. Adv Polym Sci 1994;116:207–47.

[28] Solvay-Solexis, "Galden® HT low-boiling" safety data sheets.

[29] Crank J, Park GS. Diffusion in polymers. London: Academic Press; 1986.

[30] Insight II (400P+) software package. San Diego, CA, USA: Accelrys Inc.; 2004.

[31] Maple JR, Hwang M-J, Stockfish TP, Dinur U, Waldman M, Ewig CS, et al. Derivation of class II force fields. I. Methodology and quantum force field for the alkyl functional group and alkane molecules. J Comput Chem 1994;15:162–82.
[32] Theodorou DN, Suter UW. Detailed molecular structure of a vinyl polymer glass. Macromolecules 1985;18:1467–78.
[33] Theodorou DN, Suter UW. Atomistic modeling of mechanical properties of polymeric glasses. Macromolecules 1986;19:139–54.
[34] Hofmann D, Fritz L, Ulbrich J, Shepers C, Boehning M. Detailed-atomistic molecular modeling of small molecule diffusion and solution processes in polymeric membrane materials. Macromol Theory Simul 2000;9:293–327.
[35] Tocci E, Hofmann D, Paul D, Russo N, Drioli E. A molecular simulation study on gas diffusion in a dense poly(ether-ether-ketone) membrane. Polymer 2001;42:521–33.
[36] Andrea TA, Swope WC, Andersen HC. The role of long range forces in determining the structure and properties of liquid water. J Chem Phys 1983;79:4576–84.
[37] Berendsen HJC, Postma JPM, van Gunsteren WF, DiNola A, Haak JR. Molecular dynamics with coupling to an external bath. J Chem Phys 1984;81:3684–90.
[38] Tiller AR. GSNET program. Biosym Technologies; 1993;
Tiller AR. GSDIF program. Biosym Technologies; 1993.
[39] Haile JM. Molecular dynamics simulations, elementary methods. New York: Wiley-Interscience; 1992.
[40] Mueller-Plathe F, Rogers SC, van Gunsteren WF. Computational evidence of anomalous diffusion of small molecules in amorphous polymers. Chem Phys Lett 1992;199:237–43.
[41] Gusev AA, Arizzi S, Suter UW, Moll DJ. Dynamics of light gases in rigid matrices of dense polymers. J Chem Phys 1993;99:2221–7.
[42] Gusev AA, Suter UW. Dynamics of small molecules in dense polymers subject to thermal motion. J Chem Phys 1993;99:2228–34.
[43] Gusev AA, Suter UW, Moll DJ. Relationship between helium transport and molecular motions in a glassy polycarbonate. Macromolecules 1995;28:2582–4.
[44] Gusev AA, Suter UW. A model for transport of diatomic molecules through elastic solids. J Comput Aided Mater Des 1993;1:63–73.
[45] Schneider HA. Conformational entropy contributions to the glass temperature of blends of miscible polymers. J Res Natl Inst Stand Technol 1997;102:229–48.
[46] Kwei TJ. Effect of hydrogen bonding on the glass transition temperatures of polymer mixtures. J Polym Sci Polym Lett Ed 1984;22:307–13.
[47] Kwei TK, Pearce EM, Pennacchia JR, Charton M. Correlation between the glass transition temperatures of polymer mixtures and intermolecular force parameters. Macromolecules 1987;20:1174–6.
[48] Lin AA, Kwei TK, Reiser A. On the physical meaning of the Kwei equation for the glass transition temperature of polymer blends. Macromolecules 1989;22:4112–9.
[49] Ruiz-Treviño FA, Paul DR. A quantitative model for the specific volume of polymer–diluent mixtures in the glassy state. J Polym Sci Part B Polym Phys 1998;36:1037–50.
[50] Ruiz-Treviño FA, Paul DR. Modification of polysulfone gas separation membranes by additives. J Appl Polym Sci 1997;66:1925–41.
[51] Ruiz-Treviño FA, Paul DR. Gas permselectivity properties of high free volume polymers modified by a low molecular weight additive. J Appl Polym Sci 1998;68:403–15.
[52] Fox TG. Influence of diluent and copolymer composition on the glass transition temperature of copolymers. Bull Am Phys Soc 1956;1:123–35.
[53] Solvay-Solexis, personal communication.
[54] Maeda Y, Paul DR. Effect of antiplasticization on selectivity and productivity of gas separation membranes. J Membr Sci 1987;30:1–9.
[55] Maeda Y, Paul DR. Effect of antiplasticization on gas sorption and transport. I: polysulfone. J Polym Sci Part B Polym Phys 1987;25:957–80.
[56] Maeda Y, Paul DR. Effect of antiplasticization on gas sorption and transport. II: poly(phenylene oxide). J Polym Sci B Polym Phys 1987;25:981–1003.
[57] Maeda Y, Paul DR. Effect of antiplasticization on gas sorption and transport. III: free volume interpretation. J Polym Sci Part B Polym Phys 1987;25:1005–16.
[58] Van Krevelen DW. Properties of polymers. 3rd ed. Amsterdam: Elsevier; 1990. p. 71.
[59] Hofmann D, Entrialgo-Castano M, Lerbret A, Heuchel M, Yampolskii Y. Molecular modeling investigation of free volume distributions in stiff chain polymers with conventional and ultra-high free volume: comparison between molecular modeling and positron lifetime studies. Macromolecules 2003;36:8528–38.
[60] European commission sixth framework program project MultiMatDesign. ‘‘Computer aided molecular design of multifunctional materials with controlled permeability properties’’. Contract number: NMP3-CT-2005–013644’’.
[61] Alentiev A, Yampolskii Yu, Vidyakin M, Rusanov A, Chalykh A. Fifth international symposium on ‘‘Molecular mobility and order in polymer systems’’. St. Petersburg; 2005. p. 175.